Supplemental Methods, Tables and Figures for:

Electrostatic properties of complexes along a DNA glycosylase damage search pathway

Shannen L. Cravens, Matthew Hobson, and James T. Stivers

Characterization of 1-[2-Deoxy-5-*O*-(4,4'-dimethoxytrityl)-2-fluoro-1-β-arabinofuranosyl]uracil. The identity and purity of the previously synthesized modified uracil phosphoramidite was verified by NMR and ESI mass spectrometry. All chemical shifts, splitting patterns, and relevant J-couplings were found to be consistent with what has been previously reported.[1]

^{1}H NMR (500 MHz, $CDCl_3$): δ 1.02 – 1.61 [m, 12H, 2 x $(CH_3)_2CH$]. 2.53 (two t, 2H, CH_2CH_2CN), 3.35 – 3.70 (m, 6H, H5', 5'', CH_2CH_2CN, 2 x $(CH_3)_2CH$], 4.11 – 4.19 (m, 1H, H4'), 4.49 – 4.68 (m, 1H, H3'), 5.12 and 5.25 (two m, 1H, H2', $J_{2',F}$ = 52.00 Hz), 5.59 (d, 1H, H5), 6.35 (m, 1H, H1', $J_{1'F}$ = 18.00 Hz), 6.80 – 7.50 (m, 14H, trityl), 7.59 (dd, 1H, H6, $J_{6,F}$ = 1.90 Hz), 8.55 (bs, 1H, NH).

31P NMR ($CDCl_3$, internal standard – TPPO in C_6D_6): δ 148.7 (s) and 149.3 (s), slower and faster migrating isomers, respectively.

ESI mass spectrometry: Mass determination was performed in the presence of LiCl, using methods previously described.[2,3] One prominent peak was observed with m/z = 755.12, which is consistent with the expected [M+Li](+) ion (m/z = 755.72).

Oligonucleotide Reagents

All DNA substrates listed below (except D^S) were purchased from either Integrated DNA Technologies (www.idtdna.com) or Eurofins MWG Operon (www.operon.com). Long oligos (>20 base pairs) were purified by denaturing gel electrophoresis. For all uracil containing duplex substrates the base placed opposite the uracil is specified below. All DNAs used in this study were in the duplex form and the sequences are listed below (the sequences of the complimentary strands are not indicated).

15mer-Fluorescein labeled non-specific DNA (D^N)

5′-FAM-AGG CGC ATA GTC GCA-3′

19mer-Specific DNA (D^S), U^β-G pair

5′-GCG GCC AA PU^βA AAA AGC GC-3′

(P - 2-aminopurine)

19mer-Abasic DNA (aDNA), ϕ-A pair

5′-GCG GCC AAA ϕ AA AAA GCG C-3′

(ϕ - tetrahydrofuran abasic site mimic)

30mer-Single uracil lesion (PUA-30), U-A pair

5′-CGT AGC CAC TGC AAP UAA ACA GAG CAT AGG-3′

(P - 2-aminopurine)

90mer-20 bp U separation (S20), U-A pairs

5′-GGT ATC CGC TCA CAA TTC CAC ACA ATG CTG AGG AAT CGA U AG CTA

AGT AGG ATG AAT CGA U AG CTA AGC TGA GGC ATA CAG TGT CGA GCC-3′

Supplementary Table S1. Binding affinities of hUNG and non-specific DNA ($1/K_a^N$) at variable salt concentration.

	$1/K_a^N$ (μM)		
$[K^+]$ (mM)	KCl	KGlu	KF
36	1.3 ± 0.3	1.3 ±0.3	1.3 ± 0.3
46	3.4 ± 0.3	1.2 ± 0.1	--[a]
56	5 ± 3	2.8 ± 0.7	4.3 ± 0.9
66	11.1 ± 0.9	5.7 ± 0.1	--
81	27.7 ± 0.7	7.6 ± 0.5	--
110	95 ± 5	28.1 ± 0.9	--
130	143 ± 9	50 ± 3	--
150	216 ± 8	80 ± 5	80 ± 2
170	360 ± 50	118 ± 5	--

[a] Data not collected at given salt concentration.

Supplementary Table S2. Specific DNA binding affinities ($1/K_a^S$) and association (k_{on}) and dissociation (k_{off}^S) rate constants for hUNG as a function of [K^+].[a]

[K^+] (mM)	k_{on}^S (M^{-1} s^{-1})	k_{off}^S (s^{-1})	$1/K_a^S$ (nM)[b]	k_{off}^S/k_{on}^S (nM)[c]
36	8.5 ± 0.1 x 10^8	3.8 ± 0.3	10 ± 3	4.5 ± 0.4
66	4.6 ± 0.3 x 10^8	6.4 ± 0.1	26 ± 8	14 ± 1
81	3.5 ± 0.3 x 10^8	--	--	--
110	1.8 ± 0.1 x 10^8	6.9 ± 0.5	--	40 ± 5
150	9.6 ± 0.4 x 10^7	8.7 ± 0.7	260 ± 77	91 ± 11

[a] All experiments were conducted using KGlu as the salt unless otherwise noted.

[b] K_a measured by fluorescence titration in the presence of KF.

[c] The ratio k_{off}^S/k_{on}^S was obtained from stopped-flow fluorescence measurements.

Supplementary Table S3. Steady-state kinetic parameters of hUNG and specific DNA at various salt concentrations.[a]

[K^+] (mM)	k_{cat} (s^{-1})	K_m (M)	k_{cat}/K_m (M^{-1} s^{-1})
36	3.5 ± 0.3	9 ± 3 x 10^{-8}	4 ± 2 x10^7
66	9.1 ± 0.6	3.5 ± 0.7 x 10^{-7}	2.6 ± 0.7 x10^7
110	9.1 ± 0.4	7.8 ± 0.8 x 10^{-7}	1.2 ± 0.1 x10^7
150	15 ± 2	2.5 ± 0.5 x 10^{-6}	6 ± 2 x 10^6

[a] All experiments were conducted using KGlu as the salt.

Supplementary Table S4. Probability of site transfer (P_{trans}) between two uracils with 20 base pair spacing at varying salt concentrations.[a]

$[K^+]$ (mM)	P_{trans}
13	0.36 ± 0.03
22	0.37 ± 0.02
35	0.27 ± 0.07
52	0.12 ± 0.02
63	0.09 ± 0.01

[a] All experiments were conducted using KGlu as the salt.

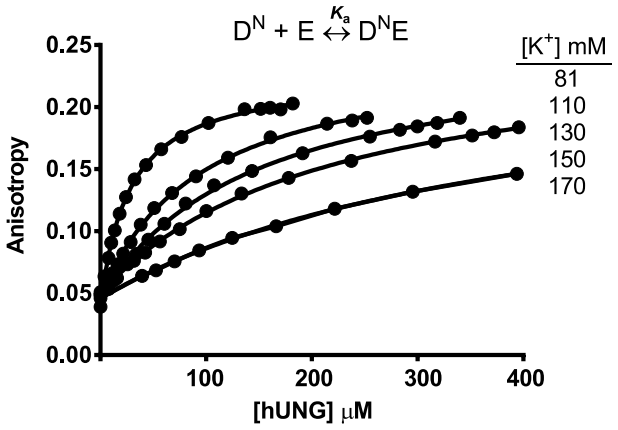

Supplementary Figure S1. Salt dependence of the non-specific DNA (D^N) equilibrium binding affinity at high salt concentrations. Changes in fluorescence anisotropy of D^N (100 nM) are plotted as a function of hUNG concentration at varying potassium ion concentrations (81 mM – 170 mM). Data presented here is an extension of the corresponding binding curves presented in Figure 2B.

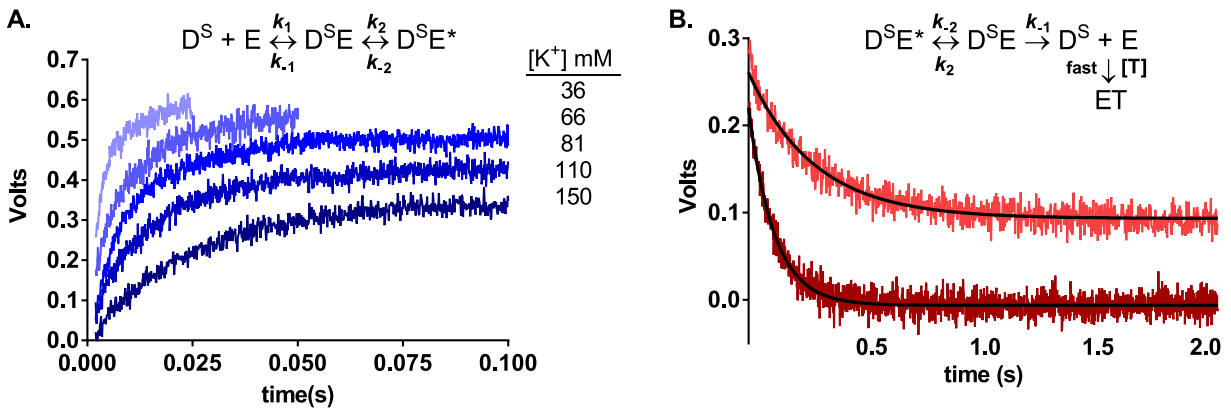

Supplementary Figure S2. Salt dependence of the association (k_{on}) and dissociation (k_{off}) kinetics of hUNG binding to specific DNA (D^S). (**A**) Raw fluorescence traces of the increase in 2-AP fluorescence upon binding of hUNG under salt concentrations of 36 – 150 mM K^+. Equal volume solutions of D^S and hUNG of equal concentration (400-600 nM) were mixed and the time dependent increase in 2-AP fluorescence was followed (λ_{ex} = 310 nm). Traces are displaced along the y-axis for ease of visualization. (**B**) Kinetic trace of the dissociation of hUNG from D^S at 36 mM K^+ (pink) and 150mM K^+(red). Data for 150 mM K^+ is the same trace presented in Figure 3D. Abasic site-containing DNA (aDNA, 5 μM) was mixed with an equal volume solution containing 0.8 μM hUNG and 0.2 μM D^S and the time dependent decrease in 2-AP fluorescence was followed (λ_{ex} = 310 nm). The lines are the best-fits to a single exponential decay. Traces are displaced along the y-axis for ease of visualization.

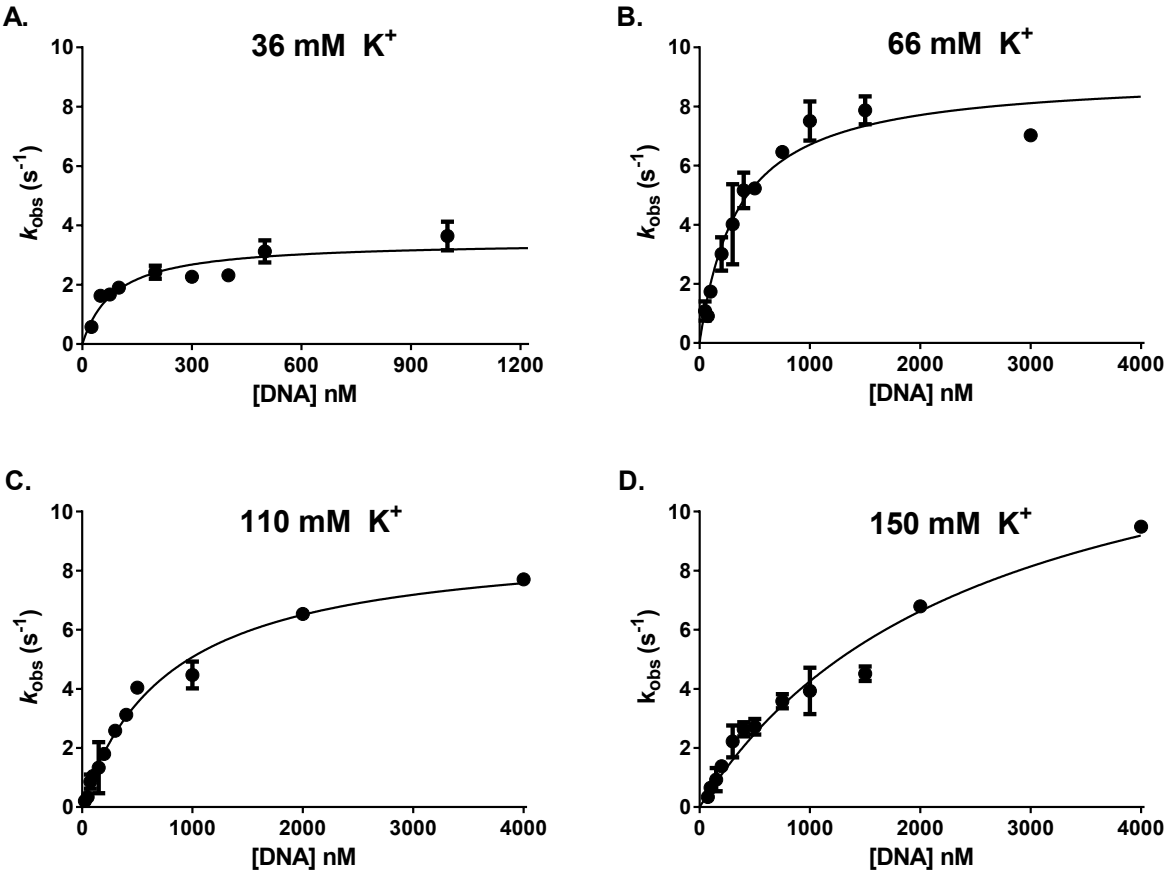

Supplementary Figure S3. Michaelis-Menten curves of the initial rates of reaction with PUA-30 as a function of DNA concentration. The various salt concentrations are indicated in each plot (**A**-**D**). For panel (**D**) we attempted to attain greater saturation of the enzyme but the DNA concentration could not be increased beyond 4 μM due to apparent substrate inhibition or aggregation at higher concentrations.

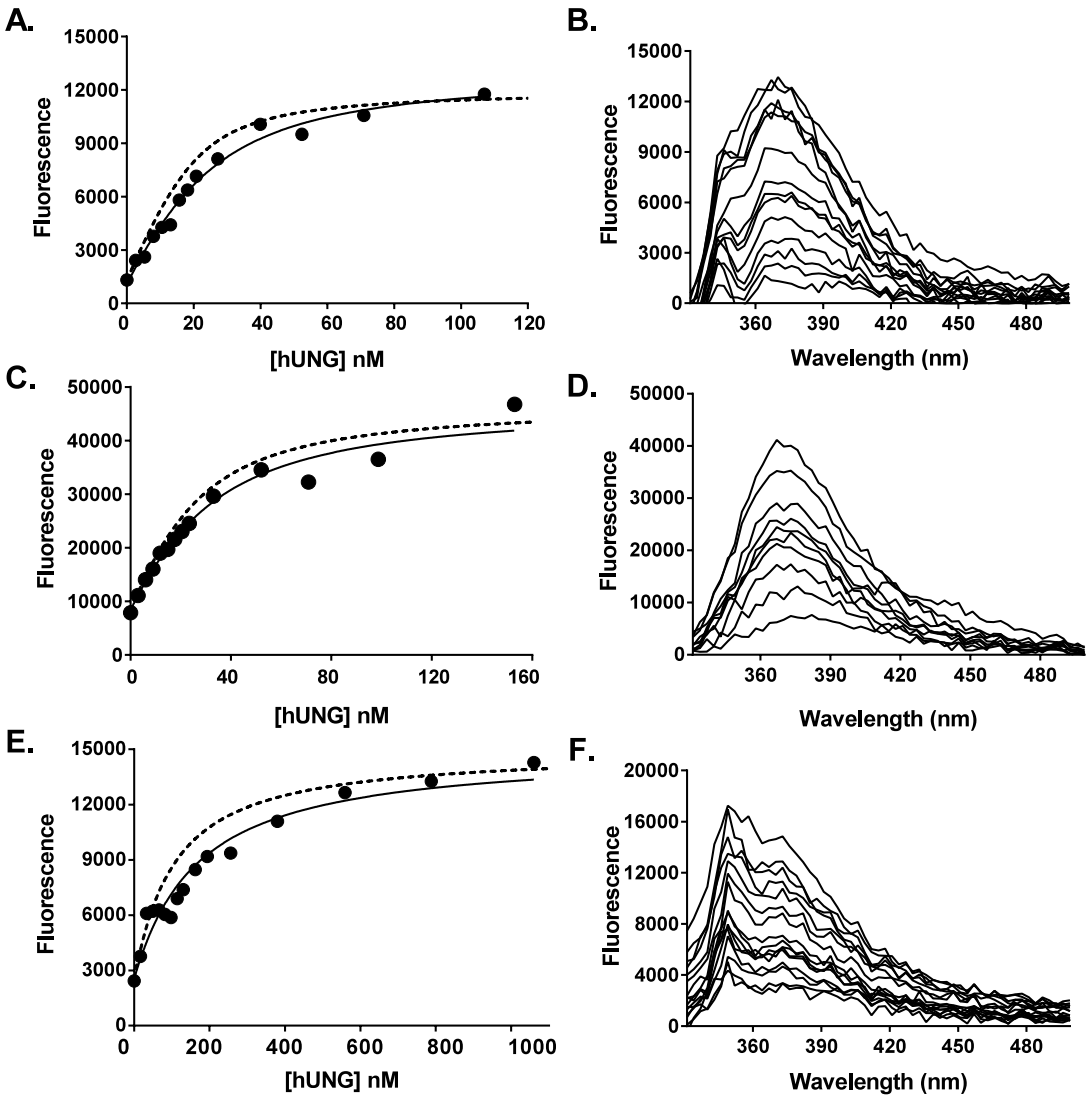

Supplementary Figure S4. Binding affinity (K_D) of the specific substrate determined by fluorescence titration at varying salt concentrations and comparison to the values determined by stopped-flow (dashed lines, k_{off}^S/k_{on}^S ratios are reported Table S2). Fluorescence intensities at 370 nm as a function of hUNG concentration (solid line) compared to the theoretical curves derived from the ratios k_{off}^S/k_{on}^S (dashed lines) in the presence of (**A**) and (**B**) 36 mM KF, (**C**) and (**D**) 66 mM KF, (**E**) and (**F**) 150 mM KF. Panels **B**, **D**, and **F** are background corrected fluorescence emission scans. The residual peak at ~330 nm is due to imperfect subtraction of the intense water Raman scattering peak when using very low DNA concentrations.

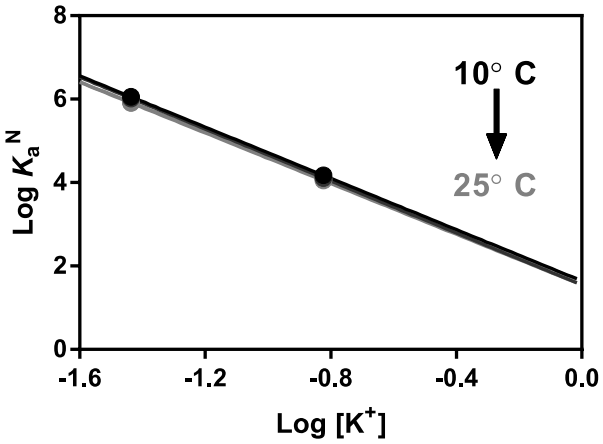

Supplementary Figure S5. Salt dependence of the non-specific DNA binding affinity is identical at 10, 15, 20, and 25°C (36 mM and 150 mM KGlu). This behavior is expected from entropically driven ion displacement.

REFERENCES

(1) Stivers, J. T., Pankiewicz, K. W., and Watanabe, K. A. (1999) Kinetic mechanism of damage site recognition and uracil flipping by Escherichia coli uracil DNA glycosylase. *Biochemistry 38*, 952–963.

(2) Kupihar, Z., Timar, Z., Dellinger, D. J., and Caruthers, M. H. (2005) Accurate mass analysis of phosphoramidites by electrospray mass spectrometry. *Nucleosides Nucleotides Nucleic Acids 24*, 663–666.

(3) Kele, Kupihar, Kovacs, Janaky, Szabo. (1999) Electrospray mass spectrometry of phosphoramidites, a group of acid-labile compounds. *J Mass Spectrom 34*, 1317–1321.